dynamic PET approach [1, 3, 4]. Also, calculations to produce parametric images of RBF has been reported [5]. However, the quantitative computation of RBF has so far assumed that the blood/tissue partition coefficient of water (p, ml/g) is uniform for the whole region of renal tissue [3, 4], and/or that the contribution of radioactivity from the vascular space is negligible [5–7]. The influence on quantitative accuracy of these assumptions is unknown.

In previous studies RBF has been computed from the uptake rate (K_1, ml/min/g) [1–7]. Some studies also simultaneously computed the partition coefficient (p) [6, 7], and the apparent p values obtained ranged between 0.52 and 0.78 ml/g. From the published values of water content for tissue (76%) and blood (81%) [8], the p value can be physiologically determined as: p_{phys}=0.94 ml/g [9]. The much smaller apparent p value might be due to the tissue mixture (or a partial volume effect) [10, 11] because of the composite structure of the kidney. The effects of the tissue mixture affect mostly K_1 and not clearance rate (k_2 min^{-1}). Therefore the clearance rate of $H_2{}^{15}O$ (k_2 min^{-1}) multiplied by p_{phys} could be used for the calculation of blood flow rather than K_1 (ml/min/g) [11] when the effect of the tissue mixture is not negligible, although it is unknown how the glomerular filtration rate (GFR) additionally contribute to k_2. Thus, the influence of GFR on k_2 should be evaluated and allowed for in the computation of RBF.

The aim of this study was to develop a method to simultaneously calculate parametric images of K_1 and k_2 as well as the arterial blood volume (V_A, ml/ml). The feasibility in terms of quantitative accuracy and image quality of calculated images was experimentally tested in healthy subjects. GFR was measured in each subject to investigate how much it contributes to the clearance rate (k_2, min^{-1}). A simulation study was also performed to evaluate error sensitivities for possible error sources.

Materials and methods

Theory

The present formula was characterized by simultaneously estimating multiple parameters of uptake rate constant (K_1, ml/min/g) and clearance rate constant (k_2 ml/g) as well as activity concentration in the arterial vascular space (V_A, ml/ml). The kinetic model for $H_2{}^{15}O$ was based on a single-tissue compartment model as follows:

$$Ci(t) = (1 - V_A) \cdot K_1 \cdot A_w(t) \otimes e^{-k2 \cdot t} + V_A \cdot A_w(t) \qquad (1)$$

where $Ci(t)$ (Bq/ml) is radioactivity concentration in a voxel of PET image, $A_w(t)$ (Bq/ml) is the arterial input function, and ⊗ indicates the convolution integral.

In the present computation, we applied a basis function method (BFM) as introduced by Koeppe et al. [12] to compute the cerebral blood flow parametric image as well as the clearance rate constant simultaneously. Gunn et al. [13] applied this method to parametric imaging of both binding potential and the delivery of ligand relative to the reference region. The computation method has also been applied to myocardial blood flow studies to compute the uptake, clearance rates and blood volume [14, 15]. The BFM procedure for the present RBF computation is illustrated in Fig. 1. The BFM method enables parametric images to be computed by using linear least squares together with a discrete range of basis functions as the parameter value for k_2 incorporating the nonlinearity and covering the expected physiological range. The corresponding basis functions formed are:

$$F(k_2, t) = A_w(t) \otimes e^{-k2 \cdot t} \qquad (2)$$

For a physiologically reasonable range of k_2, i.e. $0 < k_2 < 15.0$ ml/min/g, 1,500 discrete values for k_2 were found to

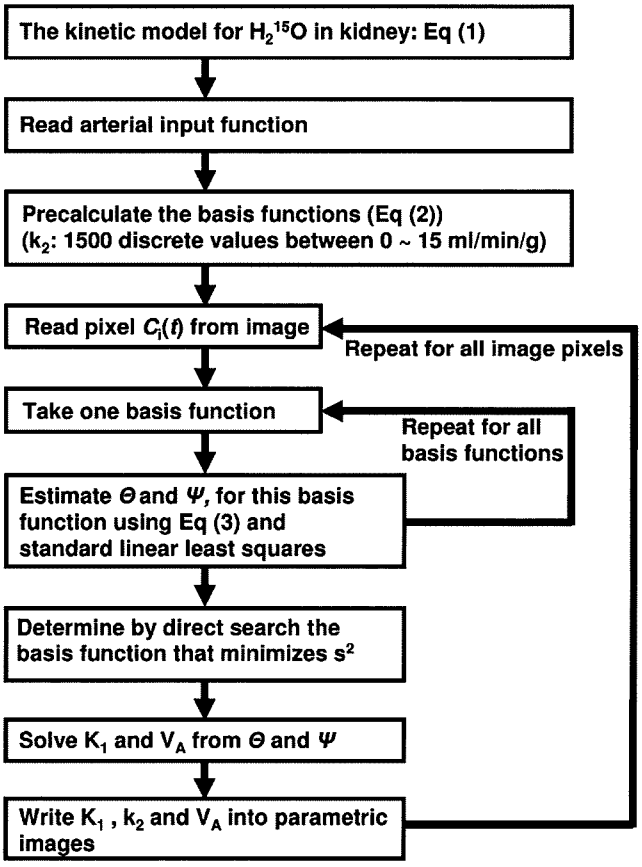

Fig. 1 Schematic diagram of the computation procedure by the BFM

be sufficient. Then Eq. 1 can be transformed for each basis function into a linear equation:

$$\begin{aligned} Ci(t) &= \Theta \cdot F(k_2, t) + \Psi \cdot A_w(t) \\ \Theta &= (1 - V_A) \cdot K_1 \\ \Psi &= V_A \end{aligned} \quad (3)$$

Hence for fixed values of k_2, the remaining two parameters Θ and Ψ can be estimated using the given basis function by standard linear least squares, and are represented as Θ_{k2} and Ψ_{k2}. The value k_2 for which the residual sum of squares

$$s(k_2)^2 = \sum_t (Ci(t) - \Theta_{k2} \cdot F(k_2, t) - \Psi_{k2} \cdot A_w(t))^2 \quad (4)$$

is minimized is determined by a direct search, and associated parameter values for this solution (K_1, k_2, V_A) are obtained.

Subjects

Six healthy human subjects (the demographics are shown in Table 1) were studied under basal conditions and stimulation (after enalapril infusion) conditions. All subjects were nonsmokers and none of them was taking any medication. All subjects gave written informed consent. The study was approved by the Ethics Committee of the Hospital District of South-Western Finland, and was conducted in accordance with the Declaration of Helsinki as revised in 1966.

Table 1 Baseline characteristics of the six subjects studied

Characteristic	Mean±SD
Age (years)	58±5
Plasma creatinine (μmol/l)	85±10
Estimated GFR (ml/min)[a]	78±4
Weight (kg)	82.8±4.5
Body mass index (kg/m^2)	26.6±2.2
Blood pressure (mmHg)	
Systolic	136±11
Diastolic	82±4
Heart rate (min^{-1})	57±5
Fasting plasma total cholesterol (mmol/l)	5.3±1.0
Fasting plasma high density cholesterol (mmol/l)	1.5±0.4
Fasting plasma triglycerides (mmol/l)	1.2±0.4
Fasting plasma low density cholesterol (mmol/l)	3.2±0.8
Blood haemoglobin (g/l)	144±12
Fasting plasma glucose (mmol/l)	5.4±0.4

[a] Estimated according to the Modification of Diet in Renal Disease study equation.

PET experiments

PET was carried out in 2-D mode using a GE Advance scanner (GE Medical Systems, Milwaukee, WI). After a 300-s transmission scan, two scans were undertaken with injection of $H_2{}^{15}O$ (1.0 to 1.5 GBq) into the cephalic vein of the right forearm. The first scan was under resting conditions and the other was under stimulated conditions, namely 20 min after infusion of 0.5 mg enalapril. The scan protocol consisted of 20 frames over a total of 240 s (15×4 s, and 5×10 s). During PET scanning, blood was withdrawn continuously through a catheter inserted into the left radial artery using a peristaltic pump (Scanditronix, Uppsala, Sweden). Radioactivity concentrations in the blood were measured with a BGO coincidence monitor system. The detectors had been cross-calibrated to the PET scanner via an ion chamber [16]. GFR was also measured in each subject [17]. To obtain the PET equivalent flow ratio for GFR, a kidney weight of 300 g and a cortex ratio of 70% were assumed [8].

Data processing

Dynamic sinogram data were corrected for dead time in each frame in addition to detector normalization. Tomographic images were reconstructed from corrected sinogram data by the OSEM method using a Hann filter with a cut-off frequency of 4.6 mm. Attenuation correction was applied with the transmission data. A reconstructed image consisted 128×128×35 matrix size with a pixel size of 4.3×4.3 mm and 4.2 mm with 20 frames. Measured arterial blood time–activity curves (TAC) were calibrated to the PET scanner and corrected for the dispersion (τ=5 and 2.5 s for intrinsic and extrinsic, respectively) [18] and delay [19]. The corrected blood TAC was used as the input function.

A set of K_1, k_2 and V_A images was generated according to the BFM formula described above, using a set of dynamic reconstructed images and input function. Computations were programmed in C environment (gcc 3.2) on a Sun workstation (Solaris 10 Sun Fire 280R) with 4 GB of memory and two Sparcv9, 900-MHz CPUs.

Data analysis

A template ROI obtained by summing whole frames of a reconstructed dynamic image was drawn on an image of the whole region of each kidney (average ROI size for the all subjects was 153±43 cm^3). Also, a ROI was drawn on a region of high tracer accumulation on the summed image as an assumed cortical region. Functional values of K_1, k_2 and V_A were extracted from both ROIs, i.e. for the whole region and the cortical region, respectively. Data re shown individually or as means±SD. Student's paired t test was

used for comparisons between the physiological states and p values <0.05 were considered significant.

The ROI for the whole region was divided plane-by-plane into subregions of ten pixels each. The subregions were created by extracting pixels first from the horizontal direction and then from the vertical direction inside the whole ROI in each slice. Each subregion consisted of a single area with the same number of pixels. Functional values of K_1, k_2 and V_A were extracted from each subregion. Tissue TACs were also obtained for each subregion from corresponding dynamic images. The three parameters K_1, k_2 and V_A were estimated using the Eq. 1 and the input function fitted to the tissue TACs by the nonlinear least-squares fitting method (NLF, Gauss-Newton method). Functional values of K_1, k_2 and V_A from corresponding subregions were then compared between the methods. Regression analysis was performed.

The model relevancy introducing p and/or V_A into the computation was tested using the Akaike Information Criterion (AIC) [20]. The most appropriate model provides the smallest AIC. The tissue TACs from the subregions were fitted and AICs were computed for models with the three parameters K_1, k_2 and V_A, fixing p ($=K_1/k_2$) at 0.35 ml/g (mean value obtained in the present subjects), fixing V_A at 0 ml/ml, and fixing V_A at 0.15 ml/ml (mean value obtained in the present subjects).

Error analysis in the simulation

Error propagation from errors in the input function for the present BFM formula was analysed for two factors: delay and dispersion in arterial TAC. It is known that the measured arterial TAC is delayed and more dispersed relative to the true input TAC in the kidney because of the time for transit of blood through the peripheral artery and the catheter tube before reaching the detector [18, 19]. Calculations of RBF so far have employed a fixed partition coefficient (p, $=K_1/k_2$, ml/g) and/or assumed the blood volume (V_A, ml/ml) as negligible throughout the whole renal region and do not estimate it regionally. BFM formulae with a fixed value of p (BFM-pfix) and blood volume V_A (BFM-vfix) in addition to the present BFM formula, and the error in these formulae, were analysed.

A typical arterial input function obtained from the present PET study was used in the present simulation as the true input function. Applying this input function to the water kinetic model in Eq. 1, a tissue TAC was created assuming values for normal kidney tissue (K_1=2.0 ml/min/g, V_A=0.14 ml/g [5], and p=0.4 ml/g, corresponding to the estimated means in cortical region in all subjects in this study).

Time in the input function was shifted from −4 to 4 s to simulate the error sensitivity due to the error in the time delay, where a positive error represents an over-correction of the time delay. The input function was convoluted or deconvoluted with a simple exponential [18] by shifting the time constant from −4 to 4 s to simulate the error sensitivity due to error in dispersion correction, where a negative error represents under-correction, as described previously [18, 21]. Values of K_1 and k_2 were calculated using simulated input functions and the tissue TACs based on the BFM formula. Errors in these calculated K_1 and k_2 values are presented as percentage differences from the assumed values. Then, the value of p was varied from 0.3 to 0.5 ml/g and the tissue TAC was generated as above to simulate the error from the value of p in BFM-pfix formula. Also, the V_A value was varied from 0.0 to 0.4 ml/ml and the tissue TAC was generated to simulating the error from V_A in BFM-vfix formula. Then, K_1 and k_2 were calculated using the true input function and the created tissue TACs, assuming p=0.4 ml/g and V_A=0.0 ml/ml in the BFM-pfix and BFM-vfix formulae, respectively. Error in K_1 and k_2 values due to fixing p is presented as the percentage difference in K_1 and k_2 as a function of p. Error in K_1 and k_2 values due to neglecting V_A is presented as the percentage difference in K_1 and k_2 as a function of V_A. Also, K_1 and k_2 were computed with V_A fixed at 0.14 ml/ml in the BFM-vfix formula from the set of the tissue TACs, in which K_1 and p were fixed at 2.0 ml/min/g and 0.4 ml/g, respectively, and V_A was varied. The percentage difference in K_1 and k_2 between the two conditions, i.e. the initial (K_1=2.0 ml/min/g and V_A=0.14 ml/ml) and changed conditions (presented as ΔK_1 and Δk_2, respectively) is presented as a function of the percentage difference in the assumed V_A from 0.14 ml/ml (ΔV) to investigate the extents to which the change in K_1 and k_2 were estimated when K_1 and k_2 were computed in the BFM-vfix formula.

Results

Experiments

The relationships of the regional ROI values of K_1, k_2 and V_A between NLF and BFM are shown in Fig. 2. The regression lines obtained were $K_{1,BFM}=0.93K_{1,NLF}-0.11$ ml/min/g (r=0.80, p<0.001), $k_{2,BFM}=0.96k_{2,NLF}-0.13$ ml/min/g (r=0.77, p<0.001), and $V_{A,BFM}=0.92V_{A,NLF}-0.00$ ml/ml (r=0.97, p<0.001), where the subscripts show the methods used for calculating the parametric values; the slopes were not significantly different from unity.

The fitted curve by the present model estimating K_1, k_2 and V_A fitted better than the other two models fixing p ($=K_1/k_2$) or V_A. An example of fitted curves is shown in Fig. 3. Also, the AIC values from three parameter fitting were the smallest for all subjects except two values for two

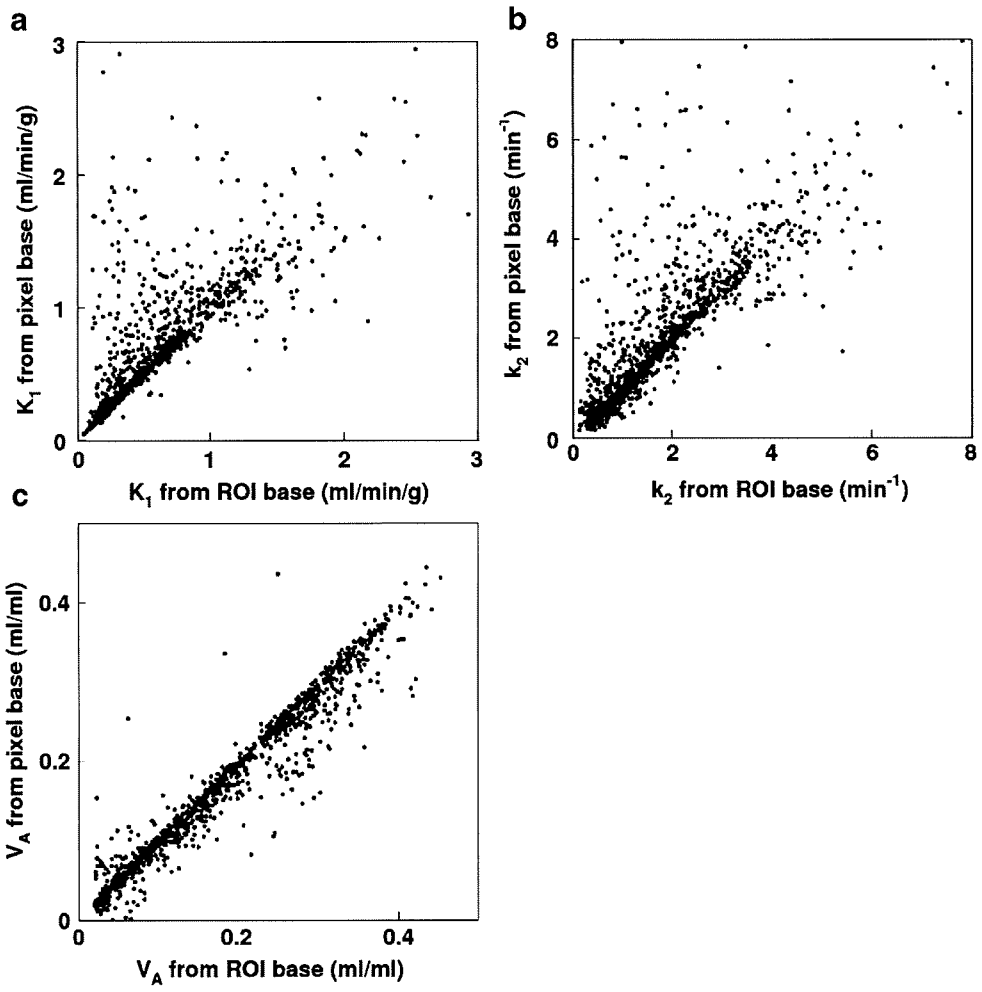

Fig. 2 Relationships of (**a**) K_1, (**b**) k_2 and (**c**) V_A between the ROI-based NLF method and pixel-based BFM. The regression lines were $K_{1,BFM}=0.93K_{1,NLF}-0.11$ ml/min/g ($r=0.80$, $p<0.001$), $k_{2,BFM}=0.96k_{2,NLF}-0.13$ ml/min/g ($r=0.77$, $p<0.001$), and $V_{A,BFM}=0.92V_{A,NLF}-0.00$ ml/ml ($r=0.97$, $p<0.001$)

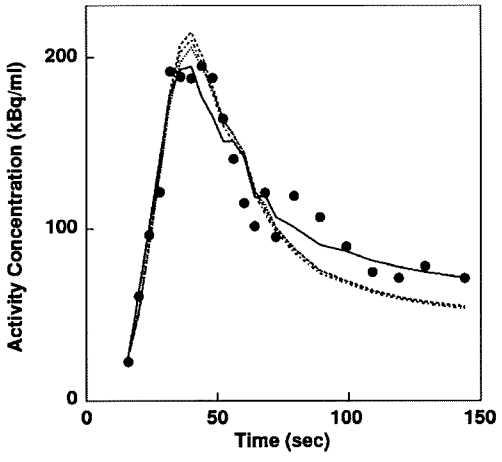

Fig. 3 Curves fitted to the measured tissue TAC from the different computation methods. Three parameters: K_1, k_2 and V_A were computed. p-fixed: K_1 and V_A were computed with p ($=K_1/k_2$) fixed at 0.35 ml/g. V_A-fixed: K_1 and k_2 were computed with V_A fixed at 0.15 ml/g. V_A-ignored: K_1 and k_2 were computed without taking into account V_A

parameter fitting fixing V_A in patient 2 and fixing p in patient 3, although some AIC values were similar (Table 2). These results show that the present method with three parameter fitting is feasible for computing RBF.

Values of K_1, $k_2 \cdot p_{phys}$ and V_A were obtained for the whole renal region and cortical region (Table 3). The K_1

Table 2 AIC values for the models

Subject	Three parameters[a]	p-fixed[b]	V_A-fixed (0.15)[c]	V_A-ignored[d]
1	484±20	519±28	499±15	494±15
2	474±9	486±14	474±9	477±8
3	525±12	523±8.3	527±10	527±7
4	483±14	497±21	501±12	506±13
5	497±18	502±19	508±32	499±13
6	496±11	507±14	500±9	497±9

[a] K_1 and k_2, V_A computed.
[b] K_1 and V_A computed with k_2 fixing such that $p=K_1/k_2=0.35$ ml/g.
[c] K_1 and k_2 computed with V_A fixed at 0.15 ml/g.
[d] K_1 and k_2 computed without taking into account V_A.

Table 3 Values of K_1, $k_2 \cdot p_{phys}$ and V_A (n=6) in the whole renal region and the cortical region calculated by the present method for the baseline conditions and the stimulated conditions

	K_1 (ml/min/g)	$k_2 \cdot p_{phys}$ (ml/min/g)	V_A (ml/ml)	GFR (ml/min/g)
Whole region				
Baseline	1.09±0.33	3.11±1.48	0.15±0.09	0.35±2[a]
Enalapril-stimulated	1.03±0.44	2.55±1.29	0.16±0.14	
Cortical region				
Baseline	1.57±0.60*	3.64±2.15*	0.18±0.12*	
Enalapril-stimulated	1.42±0.39*	3.55±1.64*	0.25±0.14*	

No significant difference was found between the baseline and stimulated conditions.
*Difference was significant between the whole and cortical regions.
[a] A kidney weight of 300 g and a cortex ratio of 70% were assumed.

values were smaller than $k_2 \cdot p_{phys}$ values and the ratio between them ranged from 0.35 to 0.45, suggesting that K_1 values underestimated RBF due to the partial volume effect. Both K_1 and $k_2 \cdot p_{phys}$ were not significantly different between the resting and stimulated conditions for the whole renal region and the cortical region, respectively, although the value of V_A was higher under the stimulated conditions than under the basal conditions. The GFR obtained was 78±4 ml/min, corresponding to a clearance rate of 0.37±0.02 ml/min/g and to 9.6% of the k_2 obtained for the cortical region under the normal conditions.

Representative K_1 and $k_2 \cdot p_{phys}$ images generated by the present method are shown in Fig. 4. The quality of the image is acceptable. The K_1 and $k_2 \cdot p_{phys}$ values ranged from 1.5 to 2.0 ml/min/g and 3.0 to 5.0 around cortical region, respectively, and some parts showed higher values than these. The average time required to compute the parametric images was 2 min 23 s.

Error analysis

The sizes of the errors introduced in both K_1 and k_2 were less than 20% for estimation of delay and the dispersion time constant up to 2 s (Fig. 5). The error sensitivity in K_1 and k_2 was 40% when the partition coefficient was 0.35 (Fig. 6). The magnitude of the error was markedly enhanced when the blood volume was ignored (Fig. 7a), and if the arterial blood volume increased by 25%, K_1 and k_2 were overestimated by 20% (Fig. 7a).

Discussion

We have presented an approach to generating quantitative K_1, k_2 and V_A images using $H_2{}^{15}O$ and PET applying the BFM computation method. The validity of this approach in healthy human subjects under resting and stimulated conditions is described. The rate constant values of K_1 and $k_2 \cdot p_{phys}$ obtained from the parametric images were consistent against NFL and the quality of the K_1 and $k_2 \cdot p_{phys}$ images obtained was acceptable. The smaller K_1 against $k_2 \cdot p_{phys}$ values suggested that the K_1 values underestimated the absolute RBF value due to the partial volume effect. The simulation showed that the delay time and dispersion time constant should be estimated within an accuracy of 2 s, and V_A and p cannot be ignored/fixed to

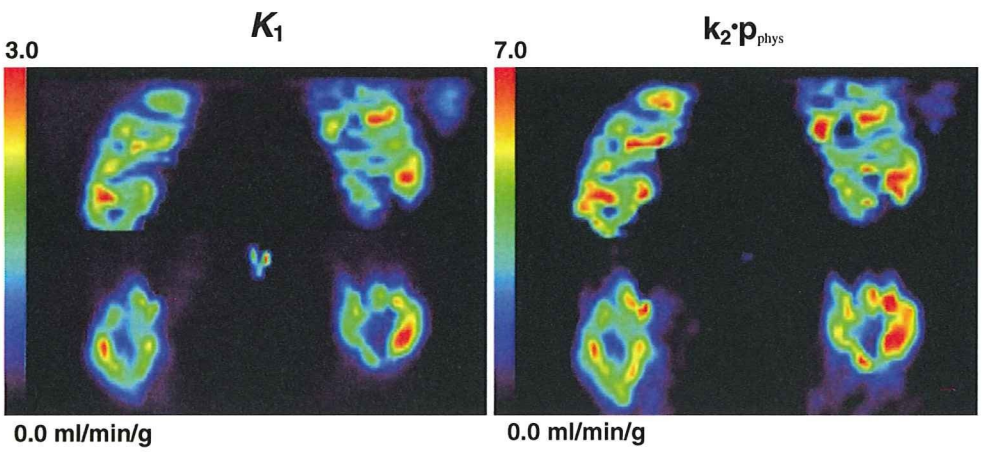

Fig. 4 Representative parametric images of K_1 (*left*) and $k_2 \cdot p_{phys}$ (*right*) for a subject under baseline conditions. Coronal (*upper*) and transverse (*lower*) views are shown

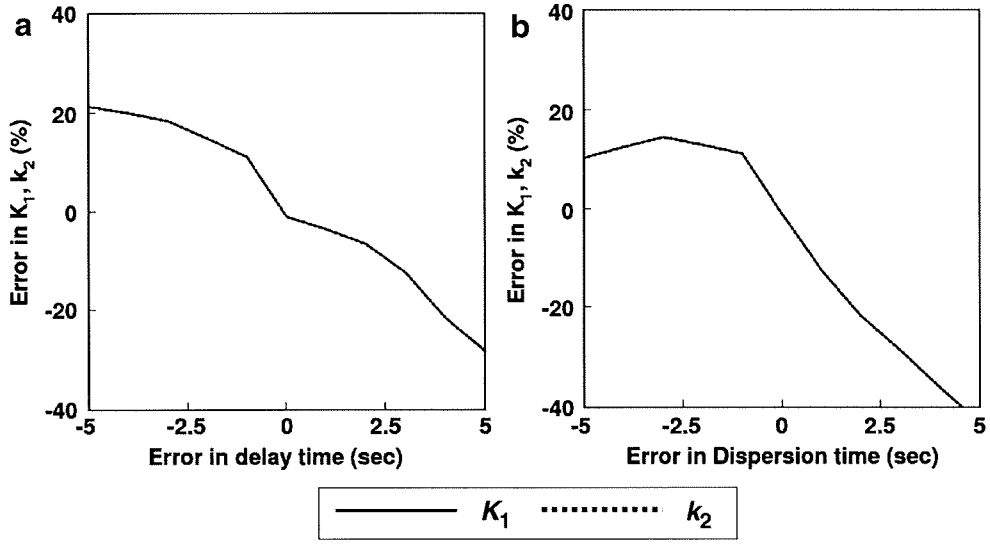

Fig. 5 Error propagation from the error in input time (**a**) and dispersion time constant (**b**) to K_1 and k_2 (the two lines were identical). Positive and negative values of error indicate over- and under-correction of delay time and dispersion time, respectively

estimate the rate constants of K_1 and/or k_2. Also V_A cannot be ignored, even when only relative rate constant values are needed. These findings suggest that the present k_2 obtained BFM technique provides an RBF image with reasonable accuracy and quality.

In the present study the rate constants of K_1 and k_2 were experimentally computed, and the ratios obtained ranged from 0.35 to 0.45 ml/g, which corresponds to the apparent kidney–blood partition coefficient. The much smaller apparent p value might be due to a partial volume effect, as has been demonstrated in a previous brain and cardiac study [10, 11], because of the composite structure of the kidney, the spatial resolution of the reconstructed image and breathing movement of the patient during the scan. When the rate constant K_1 is underestimated due to the partial volume effect, $k_2 \cdot p_{phys}$ could be applied for RBF rather than K_1. The present study showed that the contribution of GFR to the clearance rate was only 10%, and that $k_2 \cdot p_{phys}$ is more appropriate for RBF assessment, although further study of how the GFR changes under stimulated conditions is required. The $k_2 \cdot p_{phys}$ value in the cortical region obtained in the present study was 3.64±2.15 ml/min/g under normal condition, a value within the normal range of 4 to 5 ml/min/g reported in the literature [22]. Middlekauff et al. [23–25] applied the ROI base analysis, and showed similar RBF values around 4 ml/min/g. These findings also support the use of $k_2 \cdot p_{phys}$ for the calculation of RBF. The different values of RBF between the present study and the previous studies [3–5] might be due to differences in the approaches.

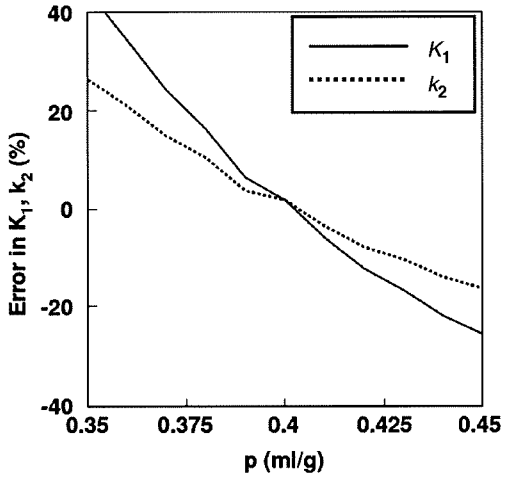

Fig. 6 Error propagation from the partition coefficient (p, ml/g) to K_1 and k_2. When the true p was varied between 0.6 and 0.8 ml/g, the size of the error in RBF was simulated assuming p=0.7 ml/g

The present computation of RBF by the BFM has two main advantages over the NLF. One is the ability to produce a voxel-by-voxel quantitative parametric map, and the other is faster computing speed. In fact, the parametric images were obtained within a reasonable time, i.e. 2.5 min with an image size of 128×128 pixels with 35 slices and 22 frames. The time could be further reduced by applying a threshold to omit pixels with lower values. From a clinical standpoint, voxel-by-voxel analysis is preferred to ROI-based analysis because the operator can independently define ROIs to improve reproducibility, and faster computations are important for analysing very large datasets.

Kinetic parameters estimated by the NLF agreed well with those estimated by the BFM as shown in Fig. 2. The disagreement in some rate constant values between the voxel-based (BFM) and ROI-based computation methods might have been due to the composite structure between the cortical region and its surroundings, or to image noise. Although superior to the NLF in terms of computing speed and ability to generate parametric maps, the BFM shares the same source of errors as the NLF because they use the

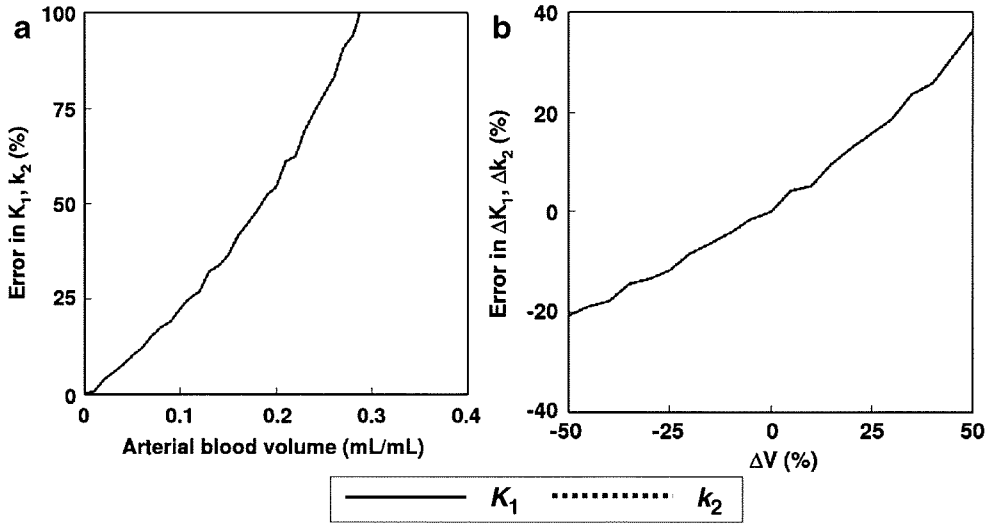

Fig. 7 **a** Error propagation from the arterial blood volume (V_A, ml/ml) to K_1 and k_2 (the two lines were identical). When the true V_A changed from 0.0 to 0.4 ml/ml, the size of the error in K_1 and k_2 calculated assuming V_A=0.0 ml/ml was simulated. **b** Error propagation from the change in arterial blood volume from 0.14 ml/ml (ΔV_A) to the change in K_1 and k_2 from the initial conditions (ΔK_1 and Δk_2, ml/min/g) (the two lines were identical)

same model and assumption. Delay and dispersion in input function, motion of the patient during a study [26–28], and flow heterogeneity [29] are sources of error for parameters estimated by both the NLF and BFM. Selection of a specific range of k_2 and the number of basis function can affect the accuracy and precision of the estimated parameters in neuroreceptor studies [30, 31]. However, the range was 0 to 15 ml/min/g in the present computation with $H_2{}^{15}O$, and the limits of this range would be acceptable for the present computation. In practice, selection of a wider range and/or a large number of discrete values of the basis function is slow and inefficient against the required accuracy and precision.

The present simulation study showed that if V_A is neglected or fixed, not only the absolute rate constants, i. e. RBF value, are overestimated, but estimated changes in RBF between two physiological states could be over- or underestimated. These findings suggest that V_A should be included to obtain either absolute or relative values of RBF. For p, the present simulation revealed that the error sensitivity in RBF for that value was significant. The values of p for the whole and cortical regions were 0.35 and 0.42 ml/g, respectively. If the value was fixed at 0.4 ml/g, a 40% overestimation in RBF for regions with a p of 0.35 occurred. Thus, regional difference in p introduce error in quantitative RBF values. Also the AIC analysis showed that introducing the extra parameters of p and V_A did not increase the AIC value against the others. These findings suggest that both p and V_A need to be estimated simultaneously with quantitative RBF, especially when changes under different conditions are assessed.

Knowledge of RBF is mostly needed in determining the severity of renovascular disease. Although the degree of renal artery stenosis is easily diagnosed, its actual effect on RBF remains difficult to quantify. In clinical work, estimates of GFR have not shown very good accuracy in relation to possible interventional treatment. Also, there is no good clinical method to easily measure single-kidney or regional RBF. We can obtain the effective renal plasma flow (ERPF) by infusing *p*-aminohippuric acid and measuring the urine and plasma concentrations, but this method only gives the total ERPF for both kidneys. An alternative is a magnetic resonance (MR) based method, which is problematic in patients with chronic kidney disease, because the contrast agent gadolinium is contraindicated in these subjects [32]. The present PET-related methodology may provide quantitative estimate of regional RBF, and be clinically applicable under conditions such as chronic allograft nephropathy and acute kidney insufficiency. The procedure – as presented here – still involves a small degree of invasiveness because of blood sampling. However, many noninvasive methods for estimating input functions have been proposed [3–5, 23–25, 33, 34], and their implementation will allow RBF to be determined in a fully noninvasive fashion, particularly for clinical purposes.

In conclusion, although some issues remain to be investigated, this study shows the feasibility of measurement of RBF using PET with $H_2{}^{15}O$.

Acknowledgments The authors thank the technical staff of the Turku PET Centre for their effort and skill dedicated to this project. This work was supported by the Hospital District of Southwest of Finland and was conducted within the "Centre of Excellence in Molecular Imaging in Cardiovascular and Metabolic Research" supported by the Academy of Finland, University of Turku, Turku University Hospital and Abo Academy. The study was further supported by grants from the Academy of Finland (206359 to P.N.), the Finnish Diabetes Foundation (P.I.), EFSD/Eli-Lilly (P.I.), the Sigrid Juselius Foundation (N.K. and P.I.), and the Novo Nordisk Foundation (P.N.).

References

1. Nitzsche EU, Choi Y, Killion D, Hoh CK, Hawkins RA, Rosenthal JT, et al. Quantification and parametric imaging of renal cortical blood flow in vivo based on Patlak graphical analysis. Kidney Int 1993;44:985–96.
2. Szabo Z, Xia J, Mathews WB, Brown PR. Future direction of renal positron emission tomography. Semin Nucl Med 2006;36:36–50.
3. Juillard L, Janier MF, Foucue D, Lionnet M, Le Bars D, Cinotti L, et al. Renal blood flow measurement by positron emission tomography using 15O-labeled water. Kidney Int 2000;57:2511–18.
4. Juillard L, Janier MF, Fouque D, Cinotti L, Maakel N, Le Bars D, et al. Dynamic renal blood flow measurement by positron emission tomography in patients with CRF. Am J Kidney Dis 2002;40:947–54.
5. Alpert NM, Rabito CA, Correia DJA, Babich JW, Littman BH, Tompkins RG, et al. Mapping of local renal blood flow with PET and H215O. J Nucl Med 2002;43:470–75.
6. Anderson HL, Yap JT, Miller MP, Robbins A, Jones T, Price PM. Assessment of pharmacodynamic vascular response in a phase I trial of combretastatin A4 phosphate. J Clin Oncol 2003;21:2823–30.
7. Anderson H, Yap JT, Wells P, Miller MP, Propper D, Price D, et al. Measurement of renal tumour and normal tissue perfusion using positron emission tomography in a phase II clinical trial of razoxane. Br J Cancer 2003;89:262–67.
8. Snyder WS, Cook MJ, Nasset ES, Karhausen LR, Howells GP, Tipton IH. Report of the Task Group on Reference Man. London: Pergamon Press; 1974. p. 175–77.
9. Herscovitch P, Raichle ME. What is the correct value for the brain–blood partition coefficient for water? J Cereb Blood Flow Metab 1985;5:65–9.
10. Iida H, Law I, Pakkenberg B, Krarup-Hansen A, Eberl S, Holm S, et al. Quantitation of regional cerebral blood flow corrected for partial volume effect using O-15 water and PET: I. Theory, error analysis, and stereologic comparison. J Cereb Blood Flow Metab 2000;20:1237–51.
11. Blomqvist G, Lammertsma AA, Mazoyer B, Wienhard K. Effect of tissue heterogeneity on quantification in positron emission tomography. Eur J Nucl Med 1995;22:652–63.
12. Koeppe RA, Holden JE, Ip WR. Performance comparison of parameter estimation techniques for the quantitation of local cerebral blood flow by dynamic positron computed tomography. J Cereb Blood Flow Metab 1985;5:224–34.
13. Gunn RN, Lammertsma AA, Hume SP, Cunningham VJ. Parametric imaging of ligand-receptor binding in PET using a simplified reference region model. Neuroimage 1997;6:279–87.
14. Watabe H, Jino H, Kawachi N, Teramoto N, Hayashi T, Ohta Y, et al. Parametric imaging of myocardial blood flow with 15O-water and PET using the basis function method. J Nucl Med 2005;46:1219–24.
15. Boellaard R, Knaapen P, Rijbroek A, Luurtsema GJ, Lammertsma AA. Evaluation of basis function and linear least squares methods for generating parametric blood flow images using 15O-water and positron emission tomography. Mol Imaging Biol 2005;7:273–85.
16. Ruotsalainen U, Raitakari M, Nuutila P, Oikonen V, Sipilä H, Teräs M, et al. Quantitative blood flow measurement of skeletal muscle using oxygen-15-water and PET. J Nucl Med 1997;38:314–19.
17. Levey A, Bosch J, Lewis J, Greene T, Rogers N, Roth D. A more accurate method to estimate glomerular filtration rate from serum creatinine: a new prediction equation. Modification of Diet in Renal Disease Study Group. Ann Intern Med 1999;130:461–70.
18. Iida H, Kanno I, Miura S, Murakami M, Takahashi K, Uemura K. Error analysis of a quantitative cerebral blood flow measurement using H215O autoradiography and positron emission tomography, with respect to the dispersion of the input function. J Cereb Blood Flow Metab 1986;6:536–45.
19. Iida H, Higano S, Tomura N, Shishido F, Kanno I, Miura S, et al. Evaluation of regional differences of tracer appearance time in cerebral tissues using [15O] water and dynamic positron emission tomography. J Cereb Blood Flow Metab 1988;8:285–88.
20. Akaike H. A new look at the statistical model identification. IEEE Trans Automat Contr 1974;AC19:716–23.
21. Kudomi N, Hayashi T, Teramoto N, Watabe H, Kawachi N, Ohta Y, et al. Rapid quantitative measurement of CMRO2 and CBF by dual administration of 15O-labeled oxygen and water during a single PET scan – a validation study and error analysis in anesthetized monkeys. J Cereb Blood Flow Metab 2005;259:1209–24.
22. Ganong WF. Review of medical physiology. 8th ed. Norwalk: Appleton & Lange; 1977. p. 522–45.
23. Middlekauff HR, Nitzsche EU, Hamilton MA, Schelbert HR, Fonarow GC, Moriguchi JD, et al. Evidence for preserved cardiopulmonary baroflex control of renal cortical blood flow in humans with advanced heart failure. Circulation 1995;92:395–401.
24. Middlekauff HR, Nitzsche EU, Hoh CK, Hamilton MA, Fonarow GC, Hage A, et al. Exaggerated renal vasoconstriction during exercise in heart failure patients. Circulation 2000;101:784–89.
25. Middlekauff HR, Nitzsche EU, Hoh CK, Hamilton MA, Fonarow GC, Hage A, et al. Exaggerated muscle mechanoreflex control of reflex renal vasoconstriction in heart failure. J Appl Physiol 2001;90:1714–19.
26. Fulton RR, Meikle SR, Eberl S, Pfeiffer J, Constable CJ. Correction for head movements in positron emission tomography using an optical motion-tracking system. IEEE Trans Nucl Sci 2002;49:116–23.
27. Bloomfield PM, Spinks TJ, Reed J, Schnorr L, Westrip AM, Livieratos L, et al. The design and implementation of a motion correction scheme for neurological PET. Phys Med Biol 2003;48:959–78.
28. Woo SK, Watabe H, Choi Y, Kim KM, Park CC, Iida H. Sinogram-based motion correction of PET images using optical motion tracking system and list-mode data acquisition. IEEE Trans Nucl Sci 2004;51:782–88.
29. Herrero P, Staudenherz A, Walsh JF, Gropler RJ, Bergmann SR. Heterogeneity of myocardial perfusion provides the physiological basis of perfusable tissue index. J Nucl Med 1995;36:320–27.
30. Cselényi Z, Olsson H, Halldin C, Gulyás B, Farde L. A comparison of recent parametric neuroreceptor mapping approaches based on measurements with the high affinity PET radioligands [11C]FLB 457 and [11C]WAY 100635. Neuroimage 2006;32:1690–708.
31. Schuitemaker A, van Berckel BN, Kropholler MA, Kloet RW, Jonker C, Scheltens P, et al. Evaluation of methods for generating parametric (R-[11C]PK11195 binding images. J Cereb Blood Flow Metab 2007;27:1603–15.
32. Martin D, Sharma P, Salman K, Jones RA, Grattan-Smith JD, Mao H, et al. Individual kidney blood flow measured with contrast-enhanced first-pass perfusion MR imaging. Radiology 2008;246:241–48.
33. Iida H, Kanno I, Takahashi A, Miura S, Murakami M, Takahashi K, et al. Measurement of absolute myocardial blood flow with H215O and dynamic positron-emission tomography strategy for quantification in relation to the partial-volume effect. Circulation 1988;78:104–15.
34. Germano G, Chen BC, Huang S-C, Gambhir SS, Hoffman EJ, Phelps ME. Use of the abdominal aorta for arterial input function determination in the hepatic and renal PET studies. J Nucl Med 1992;33:613–20.

Eur J Nucl Med Mol Imaging
DOI 10.1007/s00259-009-1262-2

ORIGINAL ARTICLE

Quantification of regional myocardial oxygen metabolism in normal pigs using positron emission tomography with injectable ^{15}O-O_2

Takashi Temma · Hidehiro Iida · Takuya Hayashi · Noboru Teramoto · Youichiro Ohta · Nobuyuki Kudomi · Hiroshi Watabe · Hideo Saji · Yasuhiro Magata

Received: 27 April 2009 / Accepted: 10 August 2009

Abstract
Purpose Although ^{15}O-O_2 gas inhalation can provide a reliable and accurate myocardial metabolic rate for oxygen by PET, the spillover from gas volume in the lung distorts the images. Recently, we developed an injectable method in which blood takes up ^{15}O-O_2 from an artificial lung, and this made it possible to estimate oxygen metabolism without the inhalation protocol. In the present study, we evaluated the effectiveness of the injectable ^{15}O-O_2 system in porcine hearts.
Methods PET scans were performed after bolus injection and continuous infusion of injectable ^{15}O-O_2 via a shunt between the femoral artery and the vein in normal pigs. The injection method was compared to the inhalation method. The oxygen extraction fraction (OEF) in the lateral walls of the heart was calculated by a compartmental model in view of the spillover and partial volume effect.
Results A significant decrease of lung radioactivity in PET images was observed compared to the continuous inhalation of ^{15}O-O_2 gas. Furthermore, the injectable ^{15}O-O_2 system provides a measurement of OEF in lateral walls of the heart that is similar to the continuous-inhalation method (0.71 ± 0.036 and 0.72 ± 0.020 for the bolus-injection and continuous-infusion methods, respectively).
Conclusion These results indicate that injectable ^{15}O-O_2 has the potential to evaluate myocardial oxygen metabolism.

Keywords Myocardial oxygen metabolism · PET · Pig · OEF · Injectable ^{15}O-O_2

T. Temma · H. Saji
Department of Patho-Functional Bioanalysis,
Graduate School of Pharmaceutical Sciences, Kyoto University,
Kyoto, Japan

H. Iida · T. Hayashi · N. Teramoto · Y. Ohta · N. Kudomi · H. Watabe
Department of Investigative Radiology,
National Cardiovascular Center Research Institute,
Osaka, Japan

Y. Magata (✉)
Laboratory of Genome Bio-Photonics,
Photon Medical Research Center,
Hamamatsu University School of Medicine,
1-20-1 Handayama,
Hamamatsu 431-3192, Japan
e-mail: magata@hama-med.ac.jp

Introduction

In the myocardium, fatty acid or glucose is used to produce energy by aerobic metabolism. Oxygen is one of the most important substrates closely related to the aerobic metabolism in the TCA cycle; thus, oxygen metabolism should be a direct reflection of myocardial metabolism of these substrates. Therefore, there has been considerable interest in the development of a method to quantify oxygen metabolism in the myocardium.

Recently, ^{11}C-acetate has been used for this purpose [1–5]. ^{11}C-acetate is taken up by the mitochondria and metabolically converted into acetyl-CoA. It then enters the TCA cycle and is transformed to ^{11}C-CO_2, which is cleared rapidly from the myocardium. Thus, the clearance pharmacokinetics reflects oxygen metabolism in the myocardium. However, the quantification of oxygen metabolism using ^{11}C-acetate is quite difficult because of various intermediary compounds.

The use of ^{15}O-O_2 gas inhalation and PET scanning can provide a quantitative myocardial metabolic rate for oxygen ($MMRO_2$) [6, 7]. The tracer kinetic model used is based on that originally proposed to describe the behavior of ^{15}O-O_2 in brain tissue [8, 9]. However, the direct translation of the

Published online: 04 September 2009

compartmental model for the brain to the heart is not permitted, because subtraction for spillover from gas volume in addition to that from the blood pool is needed. A previous study demonstrated that the gas volume can be accurately estimated from the transmission scan data; thus, this technique did not require additional emission scanning for estimating the quantitative gas volume images [6, 7]. However, gaseous radioactivity in the lung during the inhalation of ^{15}O-O_2 gas is too high in comparison to other regions. Subtraction for this contribution is straightforward and accurate using the transmission scan-derived gaseous volume images, but the lung radioactivity degraded image quality in the estimated $MMRO_2$ images.

As an alternative to gas inhalation, we recently developed a method to prepare an injectable form of ^{15}O-O_2. This was accomplished by exposing pre-collected blood to ^{15}O-O_2 gas using a small artificial lung system resulting in a maximum yield of 130 MBq/ml. We demonstrated that cerebral oxygen metabolism could be estimated in normal and ischemic rats using injectable ^{15}O-O_2 [10–12]. This technique has the potential of avoiding the inhalation protocol.

The aim of the present study was therefore to test the feasibility of using the injectable ^{15}O-O_2 oxygen system for estimating myocardial oxygen metabolism in pigs. The injection method was compared to the inhalation method to determine if the injection method resulted in a reduction of lung radioactivity, an improved image quality, a more accurate estimate of myocardial oxygen metabolism, and an improved signal-to-noise ratio.

Materials and methods

Theory

^{15}O-Oxygen was administered by IV injection or inhalation and was carried as ^{15}O-hemoglobin by blood to peripheral tissues including the myocardium, where it was converted to ^{15}O-water (^{15}O-H_2O_{met}) through aerobic metabolism. The increased distribution volume of ^{15}O-H_2O_{met}, represented by the exchangeable water space of tissue, causes delayed removal of radioactivity. This allows the definition of an appropriate model and equations to be derived for the calculation of a regional myocardial metabolic rate for oxygen ($rMMOR_2$) and regional oxygen extraction fraction (rOEF). Previous studies demonstrated that these calculations were similar to those used for estimating cerebral blood flow and oxygen metabolism and require the measurement of regional myocardial blood flow (rMBF) and a correction for spillover of activity from the vascular pools and the pulmonary alveoli [6, 7]. rMBF was measured by the ^{15}O-H_2O injection technique [13]. Activity in the vascular pools of the heart chambers and the lung was evaluated with a conventional measurement of blood volume using ^{15}O-CO, and activity in the pulmonary alveoli was evaluated with an unconventional and indirect measurement of gas volume obtained from the transmission scan. Furthermore, the existence of recirculating ^{15}O-H_2O_{met} in the blood freely accessible to the myocardium was taken into consideration.

The differential equation describing the myocardial kinetics after administration of ^{15}O-O_2 can be written as follows:

$$\frac{dC^{myo}(t)}{dt} = OEF \cdot f \cdot A_o(t) + f \cdot A_w(t) - \left(\frac{f}{p} + \lambda\right) C^{myo}(t) \quad (1)$$

where $C^{myo}(t)$ designates the true radioactivity concentration in the myocardium at time t, f is myocardial blood flow, $A_O(t)$ is the ^{15}O-O_2 radioactivity concentration in arterial blood, $A_W(t)$ is the ^{15}O-H_2O radioactivity concentration in arterial blood, p is the myocardium/blood partition coefficient of water, and λ is the physical decay constant of O-15.

Solving Eq. (1) in terms of $C^{myo}(t)$ gives:

$$C^{myo}(t) = OEF \cdot f \cdot A_o(t) * e^{-\left(\frac{f}{p}+\lambda\right)\cdot t} + f \cdot A_w(t) * e^{-\left(\frac{f}{p}+\lambda\right)\cdot t} \quad (2)$$

where the asterisk denotes the convolution integral. During steady-state conditions under the continuous administration of ^{15}O-O_2, the following relationship holds:

$$C^{myo} = \frac{OEF \cdot f \cdot A_o + f \cdot A_w}{\left(\frac{f}{p} + \lambda\right)} \quad (3)$$

In the actual PET studies, the spillover from vascular pools and pulmonary alveoli and the partial volume effect should be taken into consideration [14]. Then, the measured radioactivity concentration in the region of interest (ROI) in the myocardium ($R^{myo}(t)$) can be expressed as:

$$\begin{aligned} R^{myo}(t) = {} & \alpha \cdot C^{myo}(t) \\ & + (V_B^{myo} \cdot A_t(t) - \alpha \cdot F_{Vein} \cdot OEF \cdot A_o(t) - \alpha \cdot F_{Vein} \cdot A_w(t)) \\ & + V_G^{myo} \cdot C_{gas}(t) \end{aligned} \quad (4)$$

where α denotes the myocardial tissue fraction, V_B^{myo} is the myocardial blood volume, $A_t(t)$ is the total O-15 radioactivity concentration in arterial blood, F_{vein} is the microscopic venous blood volume, V_G^{myo} is the gas volume in the myocardial ROI and $C_{gas}(t)$ is the O-15 radioactivity concentration in V_G^{myo}.

With the bolus injection or infusion methods using an artificial lung system, the radioactivity in the pulmonary alveoli is expected to be negligible in comparison with the inhalation method. Thus, Eq. (4) can be converted to:

$$R^{myo}(t) = \alpha \cdot C^{myo}(t) + (V_B^{myo} \cdot A_t(t) - \alpha \cdot F_{Vein} \cdot OEF \cdot A_o(t) - \alpha \cdot F_{Vein} \cdot A_w(t)) \quad (5)$$

Subjects

In this study, four healthy miniature pigs (22–30 kg) were used. The pigs were anesthetized by IM injection of ketamine and xylazine followed by continuous infusion of propofol (5 mg/kg/h). The animals were then placed in the supine position on the bed of the PET scanner. All experimental procedures were approved by the local animal welfare committee.

Injectable ^{15}O-O_2 preparation

In the "injection" study, injectable ^{15}O-O_2 was used. Injectable ^{15}O-O_2 was prepared as described previously [10–12]. In brief, part of an infusion line kit (Terumo Corporation, Tokyo, Japan) and an artificial lung 18 cm in length (Senko Medical Instrument Mfg Co. Ltd., Tokyo, Japan) were connected using silicone tubing to make a closed system. Then, venous blood collected from a pig, which was used in the following PET studies, was added to the system and circulated (100 ml/min) by a peristaltic pump, followed by introduction of ^{15}O–O_2 gas (~7,000 MBq/min/433 ml) into the artificial lung for 15 min to prepare injectable ^{15}O-O_2 (5.6–60.7 MBq/ml).

In the "continuous infusion" study, the left femoral artery and right femoral vein were both cannulated. The two cannulas from the artery and the vein were connected to the opposite sides of an artificial lung to create a femoral shunt. The blood flow in the shunt was aided by a peristaltic pump (30–50 ml/min). ^{15}O-O_2 gas (~7,000 MBq/min/433 ml) was continuously introduced into the artificial lung.

PET protocol (Fig. 1)

The PET scanner was an ECAT EXACT HR (CTI/Siemens) [15], which has an imaging field of view (FOV) of 55 cm in diameter and 15 cm in axial length. The spatial resolution of the scanner is 5.8 mm in full width at half maximum at the center of the FOV.

After obtaining a 20-min transmission scan for attenuation correction and gas volume estimation, the blood pool image was obtained with a 4-min PET scan after the pigs inhaled 2.7 GBq ^{15}O-CO for 30 s. Arterial blood samples were taken every minute during the ^{15}O-CO scanning, and

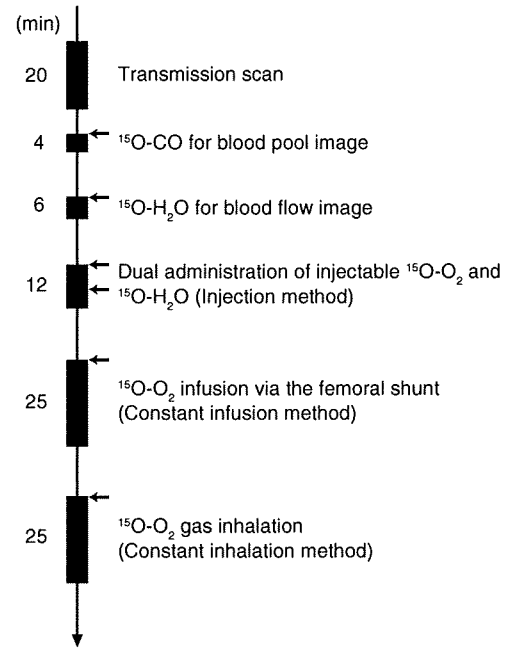

Fig. 1 Outline of the PET imaging study. The interval between scans was more than 15 min to allow for physical decay of O-15 radioactivity to background levels

the radioactivity concentration in the whole blood was measured with a NaI well-type scintillation counter calibrated against the PET scanner. Subsequently, ^{15}O-water was injected into the right femoral vein for 30 s at an infusion rate of 10 ml/min (injected radioactivity was about 1.11 GBq). Immediately after injection of ^{15}O-water, 26 dynamic frames (12×5 s, 8×15 s and 6×30 s) of PET data were acquired for 6 min.

Furthermore, two PET scans were successively performed after the IV injection of ^{15}O-O_2 (5.6–60.7 MBq/ml) for 30 s at an injection rate of 20–80 ml/min for the "injection" study, and by the continuous ^{15}O-O_2 gas infusion through the artificial lung in the femoral shunt for the "continuous infusion" study. In the "injection" study, 52 dynamic frames (12×5 s, 8×15 s, 6×30 s, 12×5 s, 8×15 s and 6×30 s) of PET data were acquired for 12 min, and 1.11 GBq of ^{15}O-water was injected IV for 30 s at 10 ml/min starting at 6 min after the administration of IV ^{15}O-O_2 according to the dual administration protocol we developed previously [16]. In the "continuous infusion" study, 26 dynamic frames (10×30 s, 5×60 s, 1×600 s and 10×30 s) were acquired for 25 min, and the 600-s frame was used for steady-state analysis.

Another PET scan was performed by ^{15}O-O_2 gas inhalation in one of the four pigs in the same protocol as the "continuous infusion" study. This was the "continuous inhalation" study. The interval between scans was more

than 15 min to allow for physical decay of O-15 radioactivity to background levels. All acquisitions were obtained in the two-dimensional mode (septa extended).

Data analysis

A filtered back-projection algorithm with a 6-mm Gaussian filter was used for image reconstruction. The reconstructed images had a matrix size of 128 × 128 × 47 and a voxel size of 1.84 × 1.84 × 3.38 mm, and all image data sets were resliced into short-axis images across the left ventricle [13].

Myocardial blood flow

rMBF was calculated from the injection of ^{15}O-H_2O by fitting the myocardial and arterial time-activity curve data to a single-tissue-compartment model that implemented corrections for partial-volume effects by introducing the tissue fraction. In addition, the model was corrected for spillover from the left ventricular (LV) chamber into the myocardial ROI by introducing the arterial blood volume [13]. In these experiments, the time-activity curves generated from large ROIs placed in the LV chamber were used as the input function.

Regional oxygen extraction fraction

In the "injection" study, rOEF was calculated according to Eqs. (2) and (5). In these formulations, F_{vein} was assumed to be 0.10 ml/g tissue and p was fixed at 0.90 ml/g. The blood volume image obtained from the ^{15}O-CO scan was used for the determination of V_B^{myo}. The value of $A_t(t)$ was obtained from the LV radioactivity concentration measured from the PET data set with small LV ROIs to minimize spillover from the myocardium. The calculation for the estimation of recirculating ^{15}O-H_2O was performed as previously described [16]. For the "continuous infusion" and "continuous inhalation" studies, in which a 600-s frame was regarded as steady-state, Eqs. (3) and (5) or Eqs. (3) and (4) were used for calculating rOEF, respectively.

Results

Table 1 summarizes the conditions of animals during the PET studies. The parameters were all within the physiologic range.

Figure 2 demonstrates the dynamic images obtained in the "injection", "continuous infusion", and "continuous inhalation" studies. With the injection and continuous-infusion methods, the right ventricle on the left side and the vena cava on the lower side were well delineated, whereas the left ventricle was moderately shown on the right side. The 16th frame (600~1,200 s after the initiation), which was used for steady-state analysis with the continuous-infusion method, was visibly distinct compared with all of the frames obtained with the injection method. However, with the continuous-inhalation method, neither ventricle could be depicted because of high radioactivity in the lung on the right and lower-side images.

The radioactivity in the blood pool obtained by ^{15}O-CO PET (Fig. 3g) and the gaseous volume estimated by inverse transmission data (Fig. 3h) were subtracted from the raw PET images (16th frame) with the continuous-inhalation and continuous-infusion methods, respectively (Fig. 3c and f). Both methods clearly delineated the myocardium after subtraction in comparison to the blood flow image (Fig. 3i). However, the continuous-inhalation method showed salient radioactivity on the lateral wall (Fig. 3c), whereas the continuous-infusion method showed only modest radioactivity in the myocardium (Fig. 3f). It is also notable that there was considerable radioactivity in the right ventricle with the continuous-infusion method even after the subtraction (Fig. 3f).

To further examine the differences between the continuous-infusion and continuous-inhalation methods, time-radioactivity curves during the PET scans were taken from four ROIs: the left ventricle (LV), right ventricle (RV), myocardium (Myo), and lung (Fig. 4). At the steady-state frame (600~1,200 s), the continuous-infusion method showed higher radioactivity in the RV and LV than in the myocardium (Fig. 4a), whereas the radioactivity of these regions was similar with the continuous-inhalation method (Fig. 4b). The radioactivity in LV was about two-thirds of that in RV in Fig. 4a, indicating that measurable radioactivity was excreted through the lung even after the femoral administration of ^{15}O-O_2. The lung excretion was also observed on the blood-subtracted image (Fig. 3e). Actually, there was significant radioactivity in the lung (Fig. 4a), although that was the lowest among the four ROIs. In contrast, the radioactivity in the myocardium was the lowest among the four ROIs with the continuous-inhalation method

Table 1 Physiological parameters of pigs during the PET studies

	pH	pCO_2 (mmHg)	pO_2 (mmHg)	tHb (g/dl)	O_2Sat (%)	HR (bpm)	BP (mmHg)	
							Diastolic	Systolic
Average	7.46	40.3	125.8	12.8	97.7	85	97.8	125.2
SD	0.032	2.51	16.69	1.30	1.83	19.5	10.4	19.3

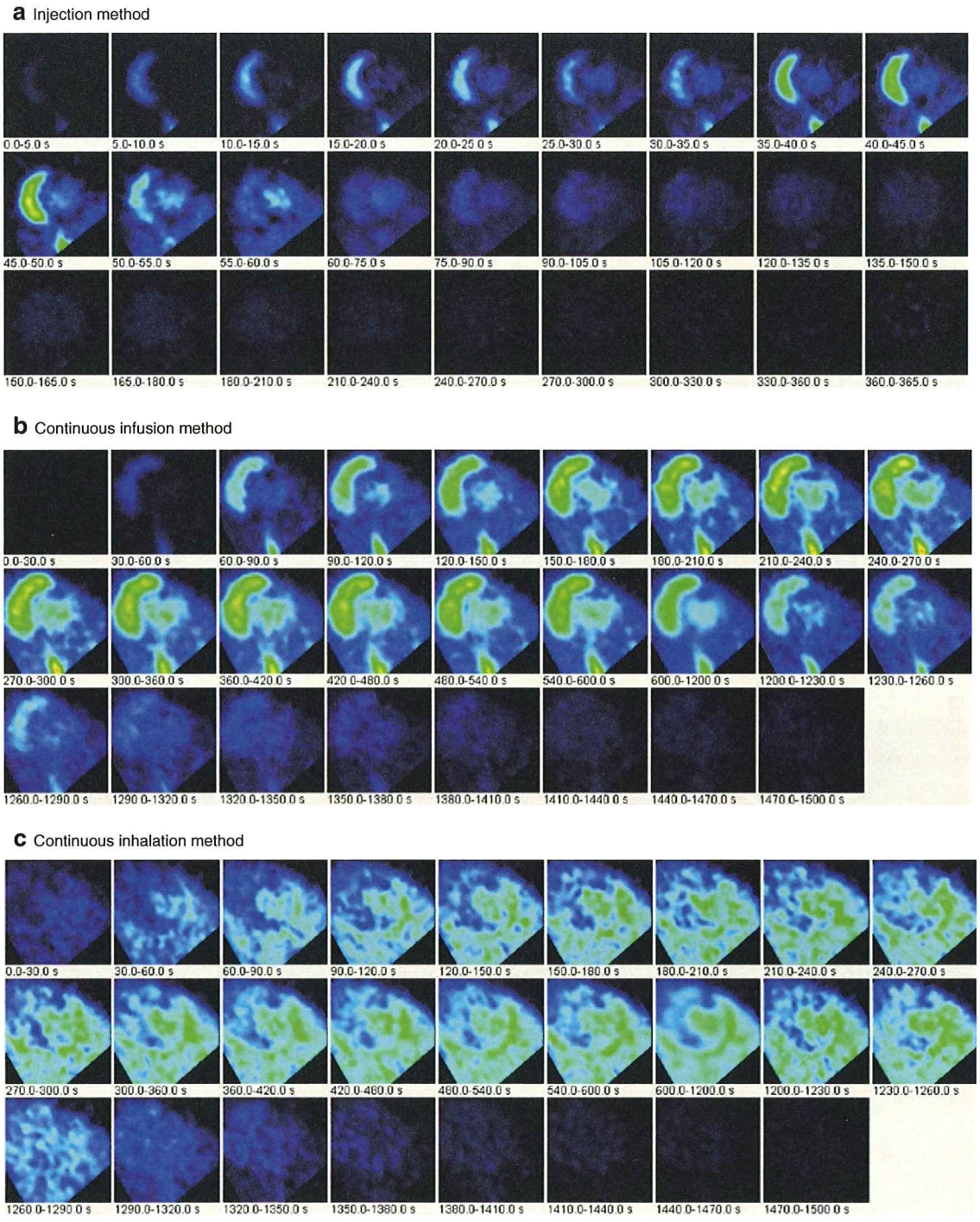

Fig. 2 PET images obtained in (**a**) the injection method, (**b**) the continuous-infusion method with injectable ^{15}O-O_2, and (**c**) the continuous-inhalation method with ^{15}O-O_2 gas

(Fig. 4b). The heart-to-lung radioactivity ratios were calculated from Fig. 4 for the quantitative estimation of image quality; the continuous-infusion method provided a ratio of 1.38±0.24, whereas the ratio was less than one with the continuous-inhalation method.

Table 2 shows the quantitative OEF values in the lateral wall obtained by the injection, continuous-infusion, and continuous-inhalation methods. These OEF values were consistent among the three methods.

Figure 5 represents the noise equivalent counts (NEC) standardized by the total counts detected by the PET scanner. Although the injection method tended to show rather high values, there was no significant difference between the values obtained by the injection and

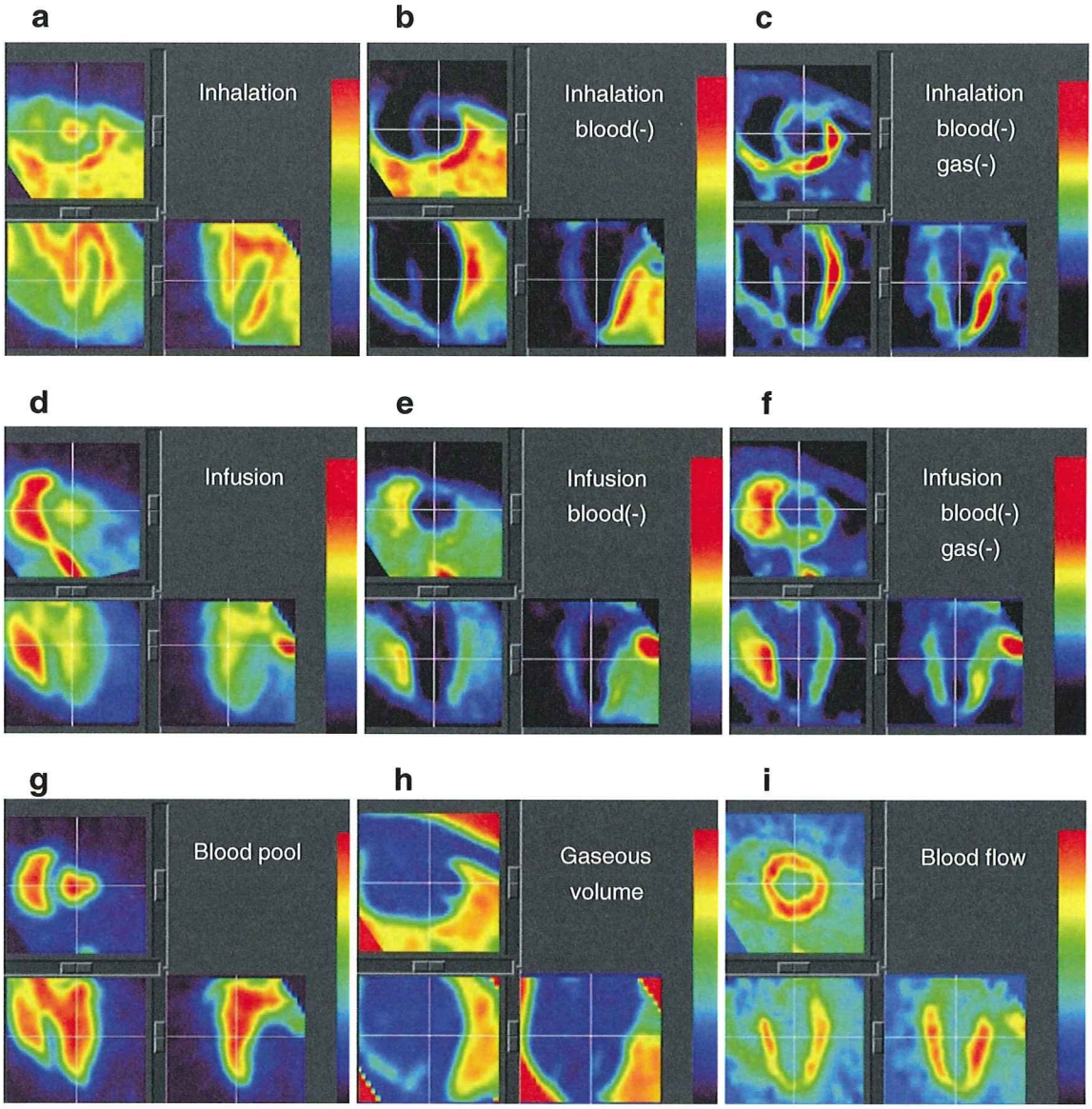

Fig. 3 PET images obtained in the study are shown. The 16th frame (steady-state frames) of the continuous-inhalation method and the continuous-infusion method are shown in (**a**) and (**d**), respectively. The 'blood-subtracted' images shown in (**b**) and (**e**) were created by subtraction of the blood-pool image by ^{15}O-CO (**g**) from (**a**) and (**d**). The 'blood- and gas-subtracted' images shown in (**c**) and (**f**) were created by the successive subtraction of the gaseous image (**h**) from (**b**) and (**e**). The myocardial blood flow image is also shown in (**i**)

continuous-infusion methods as determined by a Mann Whitney *U*-test.

Discussion

In previous studies, we showed the usefulness of the injectable ^{15}O-O_2 system for estimating cerebral oxygen metabolism in small animals such as rats under normal or ischemic conditions [10–12]. Injectable ^{15}O-O_2 replaced the inhalation protocol and radioactive ^{15}O-O_2 was administered via the tail vein. Thus, injectable ^{15}O-O_2 could abolish the artifact from the high radioactivity in the inhalation tube that distorts the PET images, especially in small animals. We considered that the concept could also be utilized in the hearts of large animals. Therefore, in the present study, we tested the feasibility of an injectable ^{15}O-O_2 system for estimating myocardial oxygen metabolism in normal pigs. In addition, since a shunt between the femoral artery and vein can be created in pigs but not in small animals, continuous infusion via the femoral shunt was also performed to achieve a constant and reliable delivery of radioactivity to the heart.

Dynamic PET scans showed a large difference in the radioactivity distribution among the three methods. Since the labeling efficiency to prepare injectable ^{15}O-O_2 was

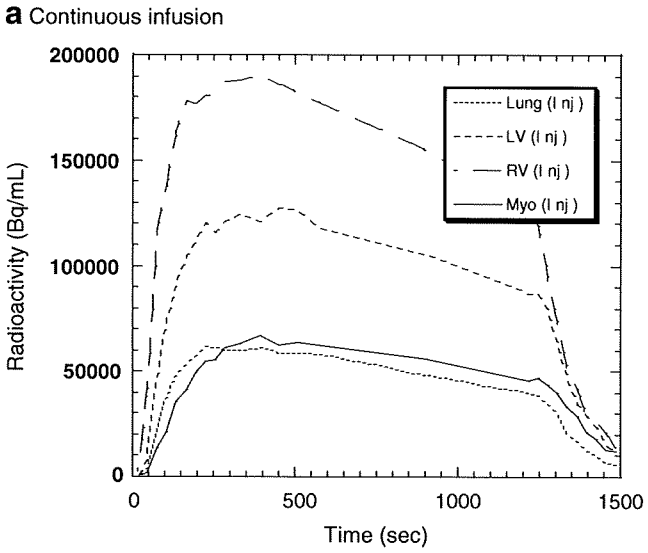

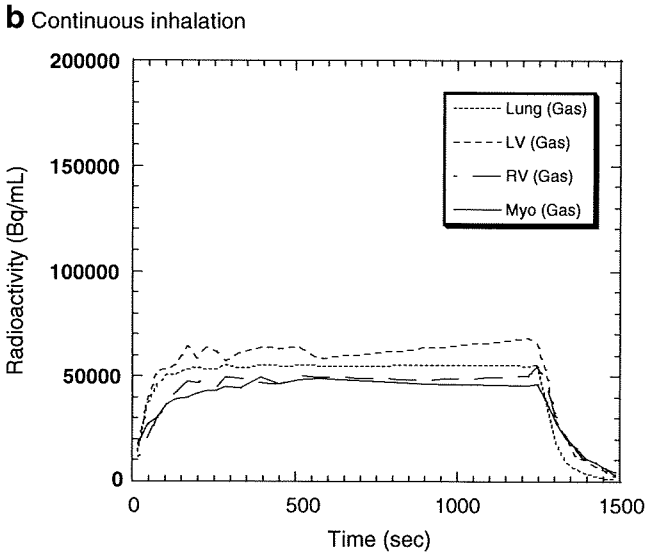

Fig. 4 Time-activity curves from the left ventricle (*LV*), the right ventricle (*RV*), the myocardium (lateral wall, Myo) and a lung region with the continuous-infusion method (**a**) and the continuous-inhalation method (**b**). The supply of radioactivity was started at time 0 s and stopped at 1,200 s. The 16th frame for the steady-state analysis was 600–1,200 s

lower with pig blood (ca. 61 MBq/ml at most) than with the blood of rats and humans (130 MBq/ml), the injection method provided rather obscure images. With the injection and continuous-infusion methods, the radioactivity in the lung was dramatically reduced in comparison to the continuous-inhalation method, since the heart-to-lung ratio with the continuous-infusion method was about 40% higher than with the continuous-inhalation method. This finding suggested that the two methods that inject radioactivity via a vein are more useful for analyzing myocardial oxygen metabolism in pigs than the continuous-inhalation method. However, a distinct difference between radioactivity of the right and left ventricles was observed in the images and time-radioactivity curves after venous administration of ^{15}O-O_2, indicating a certain degree of excretion of the radioactivity by the lung. Therefore, the spillover from the pulmonary alveoli to the myocardium could not be omitted in the two methods with venous administration, and Eq. (4) was used for the OEF analysis, although the radioactivity in the lung was lower than that in the myocardium.

On the other hand, with the continuous-inhalation method, the radioactivity of the lung was in between the radioactivity in the RV and LV. This is curious because O-15 radioactivity was supplied from the inhalation tube and transferred from the lung to blood so that the radioactivity in the lung should have been the highest among the four ROIs. This may have been caused, in part, by inhomogeneous distribution of the radioactivity in the lung due to its structure in comparison with the myocardium and ventricles, and/or by artifacts from the lung to other

Table 2 OEF estimated by the three methods using injectable ^{15}O-O_2 or ^{15}O-O_2 gas

	OEF		
	Injection	Infusion	Inhalation
Pig. 1	0.70	0.72	
Pig. 2	0.67	0.72	
Pig. 3	0.71	0.74	
Pig. 4	0.76	0.69	0.72
Average	0.71	0.72	0.72
SD	0.036	0.020	

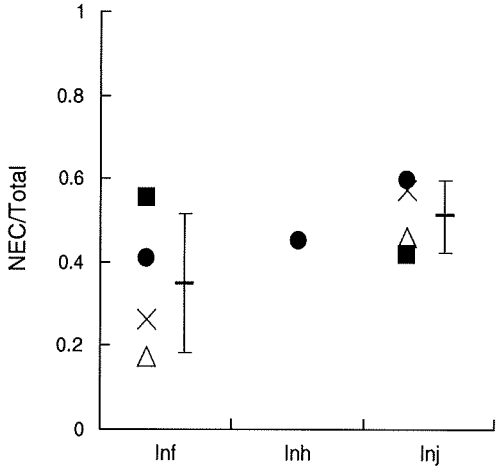

Fig. 5 The ratio of noise equivalent counts (*NEC*) to total counts in the total field of view of the PET scanner obtained with the continuous-infusion method (*Inf*), the continuous-inhalation method (*Inh*) and the injection method (*Inj*)

tissues. In any case, it is notable that the radioactivity in the myocardium was the lowest with the continuous-inhalation method, leading to difficulty in analyzing myocardial oxygen metabolism.

The OEF values in lateral walls were calculated to compare the ability of the three methods to determine myocardial oxygen metabolism by using the blood flow derived from the dual-administration protocol with the injection method and the single-administration protocol with the two continuous methods. There was no difference in the blood flow between the two protocols. Consequently, the three methods provided the same OEF value of about 0.7 and this is a physiological value in normal pigs, as was previously demonstrated [17, 18]. We have demonstrated the potential of the injectable ^{15}O-O_2 system for the estimation of physiological cerebral oxygen metabolism in rats and monkeys during early and late ischemia, hypertension, and ischemia plus hypertension [10–12, 19]. Therefore, we believe that the injection and continuous-infusion methods provide a physiological OEF in the myocardium. Nevertheless, we recognize the necessity to evaluate the reliability and usefulness of the injectable ^{15}O-O_2 method in myocardial applications. Further studies using pathophysiological animal models are required in the future, such as myocardial ischemia, hypoxia, and heart failure. On the other hand, since $MMRO_2$ is basically regarded as the product of MBF and OEF, the results indicated that these three methods were equivalent in their ability to quantify $MMRO_2$ in normal pigs, at least in the lateral wall. Although the images after the subtraction of spillovers from blood and gas showed different contrast between the continuous-infusion and continuous-inhalation methods, the ability of these two methods to measure OEF and $MMRO_2$ in the lateral walls was equivalent.

We did not evaluate myocardial oxygen metabolism in other heart regions since the radioactivity in the right ventricle could not be removed due to a significant difference of radioactivity between the ventricles with the continuous-infusion method. The injection method might be able to evaluate oxygen metabolism in other regions besides the lateral wall, although this was not evaluated in this study due to the low radioactivity of injectable ^{15}O-O_2 as described above. In the injection method, O-15 radioactivity was delivered from the femoral vein to RV, the lung, LV, and finally the myocardium. Thus, when the LV and myocardial activity reach a maximum, the RV activity is expected to be low. The later frames of the dynamic PET images with the injection method might avoid the high RV activity and delineate the myocardium and LV more clearly. With accurate anatomical information by gated PET/CT, the injection method will provide oxygen metabolism in other heart regions. In addition, the injection method has a benefit in that it is noninvasive and shortens the acquisition time in comparison with the continuous-infusion method. Future studies are needed to determine whether the injectable ^{15}O-O_2 system can be used in other heart regions.

With the injection method, the ratio of noise equivalent counts (NEC) to total counts tended to be the higher, probably because of the absence of high radioactivity adjacent to the PET scanner. Nevertheless, the continuous-infusion method did not show this tendency. This may be because tubes for the input to the artificial lung were positioned at the femoral shunt and the output to the drain of O-15 gas was positioned alongside the PET scanner, resulting in an increase of random counts during the study. Also, it is notable that the value with the continuous-inhalation method was not small, which suggests that the inhalation protocol itself did not worsen the results, but rather the high radioactivity in the lung might affect the analysis. In any case, if more care is given to shielding of the radioactivity in tubes and/or for arrangement of instruments in the PET room, a higher value of NEC/total counts will be obtained with the injectable ^{15}O-O_2 system.

The declining slope delineated in the time-activity curves with the continuous-infusion method requires some explanation. Since the flow rate of O-15 gas supply to the artificial lung positioned at the femoral shunt was maintained constant during the PET scan, it is possible that a decrease of labeling efficiency of the artificial lung occurred due to the deposition of any components of blood. The blood of rats or humans was negligibly deposited in the artificial lung during circulation at the same rate for at least 30 min in our other experiments, so that this problem may be specific for pigs. It is unclear which component in pig blood was exactly involved in the deposition and three of four pigs did not show a declining slope of the time-activity curve.

In practice, in routine studies on myocardial oxygen metabolism using large animals such as pigs, the continuous-inhalation method with ^{15}O-O_2 gas may be easier to perform for the following reasons: (1) the intubation tube used for gas anesthesia prior to the PET scan can also be used for ^{15}O-O_2 gas inhalation; (2) catheterization of the femoral artery and vein to create the femoral shunt for the continuous-infusion method may be troublesome; and (3) the injection of ^{15}O-O_2 requires an artificial lung, preparation time, and blood taken from the same animal prior to the PET scan. However, the injection of ^{15}O-O_2 has a substantial advantage over the continuous-inhalation method in that there is reduced radioactivity in the lung and clearer images of the heart are obtained. Therefore, the method for estimating myocardial oxygen metabolism should be selected depending on the objectives of the study and the surgical procedures. Furthermore, since radioactivity administered into the femoral vein is partially excreted into expired air, the injectable ^{15}O-O_2 system might be used for evaluating pulmonary function in the future.

Conclusion

In this study, we tested the feasibility of using an injectable ^{15}O-O_2 system to estimate myocardial oxygen metabolism in pigs. Both the bolus-injection and continuous-infusion methods reduced the radioactivity in the lung and provided similar OEF values in the lateral walls of the heart. These findings indicate that the injectable ^{15}O-O_2 system has the potential to evaluate myocardial oxygen metabolism.

References

1. Ohtake T. The review of myocardial positron emission computed tomography and positron imaging by gamma camera. Kaku Igaku. 1998;35:179–87.
2. Klein LJ, Visser FC, Knaapen P, Peters JH, Teule GJ, Visser CA, et al. Carbon-11 acetate as a tracer of myocardial oxygen consumption. Eur J Nucl Med. 2001;28:651–68.
3. Schelbert HR. PET contributions to understanding normal and abnormal cardiac perfusion and metabolism. Ann Biomed Eng. 2000;28:922–9.
4. Visser FC. Imaging of cardiac metabolism using radiolabelled glucose, fatty acids and acetate. Coron Artery Dis. 2001;12(Suppl 1):S12–8.
5. Hata T, Nohara R, Fujita M, Hosokawa R, Lee L, Kudo T, et al. Noninvasive assessment of myocardial viability by positron emission tomography with ^{11}C acetate in patients with old myocardial infarction. Usefulness of low-dose dobutamine infusion. Circulation. 1996;94:1834–41.
6. Yamamoto Y, de Silva R, Rhodes CG, Iida H, Lammertsma AA, Jones T, et al. Noninvasive quantification of regional myocardial metabolic rate of oxygen by $^{15}O_2$ inhalation and positron emission tomography. Experimental validation. Circulation. 1996;94:808–16.
7. Iida H, Rhodes CG, Araujo LI, Yamamoto Y, de Silva R, Maseri A, et al. Noninvasive quantification of regional myocardial metabolic rate for oxygen by use of $^{15}O_2$ inhalation and positron emission tomography. Theory, error analysis, and application in humans. Circulation. 1996;94:792–807.
8. Shidahara M, Watabe H, Kim KM, Oka H, Sago M, Hayashi T, et al. Evaluation of a commercial PET tomograph-based system for the quantitative assessment of rCBF, rOEF and $rCMRO_2$ by using sequential administration of ^{15}O-labeled compounds. Ann Nucl Med. 2002;16:317–27.
9. Mintun MA, Raichle ME, Martin WR, Herscovitch P. Brain oxygen utilization measured with O-15 radiotracers and positron emission tomography. J Nucl Med. 1984;25:177–87.
10. Magata Y, Temma T, Iida H, Ogawa M, Mukai T, Iida Y, et al. Development of injectable O-15 oxygen and estimation of rat OEF. J Cereb Blood Flow Metab. 2003;23:671–6.
11. Temma T, Magata Y, Kuge Y, Shimonaka S, Sano K, Katada Y, et al. Estimation of oxygen metabolism in a rat model of permanent ischemia using positron emission tomography with injectable ^{15}O-O_2. J Cereb Blood Flow Metab. 2006;26:1577–83.
12. Temma T, Kuge Y, Sano K, Kamihashi J, Obokata N, Kawashima H, et al. PET O-15 cerebral blood flow and metabolism after acute stroke in spontaneously hypertensive rats. Brain Res. 2008;1212:18–24.
13. Watabe H, Jino H, Kawachi N, Teramoto N, Hayashi T, Ohta Y, et al. Parametric imaging of myocardial blood flow with ^{15}O-water and PET using the basis function method. J Nucl Med. 2005;46:1219–24.
14. Iida H, Rhodes CG, de Silva R, Yamamoto Y, Araujo LI, Maseri A, et al. Myocardial tissue fraction–correction for partial volume effects and measure of tissue viability. J Nucl Med. 1991;32:2169–75.
15. Wienhard K, Dahlbom M, Eriksson L, Michel C, Bruckbauer T, Pietrzyk U, et al. The ECAT EXACT HR: performance of a new high resolution positron scanner. J Comput Assist Tomogr. 1994;18:110–8.
16. Kudomi N, Hayashi T, Teramoto N, Watabe H, Kawachi N, Ohta Y, et al. Rapid quantitative measurement of $CMRO_2$ and CBF by dual administration of ^{15}O-labeled oxygen and water during a single PET scan-a validation study and error analysis in anesthetized monkeys. J Cereb Blood Flow Metab. 2005;25:1209–24.
17. Alders DJ, Groeneveld AB, de Kanter FJ, van Beek JH. Myocardial O_2 consumption in porcine left ventricle is heterogeneously distributed in parallel to heterogeneous O_2 delivery. Am J Physiol Heart Circ Physiol. 2004;287:H1353–61.
18. Van Woerkens EC, Trouwborst A, Duncker DJ, Koning MM, Boomsma F, Verdouw PD. Catecholamines and regional hemodynamics during isovolemic hemodilution in anesthetized pigs. J Appl Physiol. 1992;72:760–9.
19. Temma T, Magata Y, Iida H, Hayashi T, Ogawa M, Mukai T, et al. Development of injectable O-15 oxygen and its application for estimation of OEF. International Congress Series, Quantitation in Biomedical Imaging with PET and MRI Proceedings of the International Workshop on Quantitation in Biomedical Imaging with PET and MRI. 2004;1265:262–65.

Journal of Cerebral Blood Flow & Metabolism (2009), 1–11

www.jcbfm.com

Measurement of density and affinity for dopamine D_2 receptors by a single positron emission tomography scan with multiple injections of [^{11}C]raclopride

Yoko Ikoma[1,2], Hiroshi Watabe[1], Takuya Hayashi[1], Yoshinori Miyake[1], Noboru Teramoto[1], Kotaro Minato[2] and Hidehiro Iida[1]

[1]*Department of Investigative Radiology, National Cardiovascular Center Research Institute, Osaka, Japan;* [2]*Biomedical Imaging and Informatics, Graduate School of Information Science, Nara Institute of Science and Technology, Nara, Japan*

Positron emission tomography (PET) with [^{11}C]raclopride has been used to investigate the density (B_{max}) and affinity (K_d) of dopamine D_2 receptors related to several neurological and psychiatric disorders. However, in assessing the B_{max} and K_d, multiple PET scans are necessary under variable specific activities of administered [^{11}C]raclopride, resulting in a long study period and unexpected physiological variations. In this paper, we have developed a method of multiple-injection graphical analysis (MI-GA) that provides the B_{max} and K_d values from a single PET scan with three sequential injections of [^{11}C]raclopride, and we validated the proposed method by performing numerous simulations and PET studies on monkeys. In the simulations, the three-injection protocol was designed according to prior knowledge of the receptor kinetics, and the errors of B_{max} and K_d estimated by MI-GA were analyzed. Simulations showed that our method could support the calculation of B_{max} and K_d, despite a slight overestimation compared with the true magnitudes. In monkey studies, we could calculate the B_{max} and K_d of diseased or normal striatum in a 150 mins scan with the three-injection protocol of [^{11}C]raclopride. Estimated B_{max} and K_d values of D_2 receptors in normal or partially dopamine-depleted striatum were comparable to the previously reported values.
Journal of Cerebral Blood Flow & Metabolism advance online publication, 11 November 2009; doi:10.1038/jcbfm.2009.239

Keywords: [^{11}C]raclopride; dopamine D_2 receptors; graphical analysis; multiple injections; positron emission tomography

Introduction

Positron emission tomography (PET) with [^{11}C]raclopride has been widely used to investigate the availability of striatal dopamine D_2 receptors *in vivo* (Farde *et al*, 1985; Köhler *et al*, 1985; Hall *et al*, 1988). A number of postmortem studies have shown that the abundance of dopamine D_2 receptor is elevated in striatum samples from untreated patients with Parkinson's disease (Guttman and Seeman, 1985; Seeman *et al*, 1987) and in schizophrenic patients who had never taken antipsychotics (Cross *et al*, 1981; Joyce *et al*, 1988). The PET measurements have made it possible to quantify *in vivo* the density and apparent affinity of receptors by systematically varying the specific activity (or mass) of an administered radioligand (see for example, Farde *et al*, 1986). A study of Parkinson's disease by Rinne *et al* (1995) with *in vivo* PET showed increased density and unchanged affinity of dopamine D_2 receptors in the putamen in comparison with healthy controls. In corresponding studies of schizophrenia, early findings with [^{11}C]*N*-methylspiperone indicated elevated D_2 binding, which was not replicated in some subsequent studies with [^{11}C]raclopride (Wong *et al*, 1986; Farde *et al*, 1987, 1990). Dysfunction of dopamine receptors has also been suggested in other neurodegenerative or psychiatric diseases (e.g., multiple-system atrophy, progressive supranuclear palsy, and attention-deficit hyperactivity disorders); however, there have been only a few studies that

Correspondence: Dr H Watabe, Department of Investigative Radiology, National Cardiovascular Center Research Institute, 5-7-1, Fujishirodai, Suita, Osaka 565-8565, Japan.
E-mail: watabe@ri.ncvc.go.jp
Received 11 September 2009; revised 13 October 2009; accepted 19 October 2009

examined receptor function directly related to density and affinity. This might be due to the inherent difficulty in measuring absolute receptor abundance based on PET recordings.

In PET scans, to determine the density and affinity of receptors directly as parameters of kinetic model, it is necessary to apply a compartmental analysis based on a two-tissue compartment five-parameter model including density of receptors B_{max} (pmol/mL), bimolecular association rate constant k_{on} (mL/pmol/min), and unimolecular dissociation rate constant k_{off} (min^{-1}) (Farde *et al*, 1989). However, since data from a single PET scan are not enough to determine the B_{max} and k_{on} individually, multiple PET scans should be taken with different molar amounts of injected ligand. In addition, model parameters are estimated by a nonlinear least squares fitting with the metabolite-corrected plasma input function, so the solutions are often unstable and sensitive to statistical noise, and invasive arterial sampling is required to use this method.

Farde *et al* (1986, 1989) determined the value of B_{max} and apparent affinity K_d ($=k_{off}/k_{on}$) by a graphical analysis using a time-activity curve (TAC) of the specifically bound target region and a reference region where specific bindings are negligible. In this method, the ratio of specific bound and free ligand concentrations at the equilibrium state are plotted versus the concentration of specific bound ligand, and B_{max} and K_d are estimated from the slope and intercept of the regression line. Other groups also used the value of distribution volume ratio − 1 estimated from the graphical analysis of Logan *et al* (1996), instead of the ratios of specific bound and free concentration, to obtain stable values of the *y*-axis quantity (Logan *et al*, 1997; Doudet and Holden, 2003; Doudet *et al*, 2003). These methods are practical, because they do not require arterial blood sampling, and their respective estimation processes are easy to carry out. However, to estimate the regression line of a graphical plot, multiple PET scans (at least two or three) are required under variable molar amounts of administered ligand, so scans have been performed on separate days. Even in quantitative PET scans, the separate day protocol may suffer from interday or intraday variations in physiologic conditions, such as cerebral blood pressure, flow, and receptor bindings, which may affect the accuracy of the estimates.

We developed a method, called the multiple-injection simplified reference tissue model (MI-SRTM), to measure the change in binding potential ($BP_{ND}=k_3/k_4$ (Mintun *et al*, 1984)) of dopamine D_2 receptors from a single session of PET scanning with multiple injections of [^{11}C]raclopride (Watabe *et al*, 2006; Ikoma *et al*, 2009), and we showed that this method could detect the change in BP_{ND} because of an increase in mass of administered [^{11}C]raclopride in a short scanning period, which is a prerequisite for measuring the saturation binding parameters as steady state. In this study, we extend our earlier report for estimating B_{max} and K_d from a single session of PET scanning with triple injections of [^{11}C]raclopride using MI-SRTM and the graphical analysis, and we validated the proposed method by performing numerous simulations and studies on monkeys using PET and [^{11}C]raclopride.

Materials and methods

Theory

Graphical Analysis with a Reference Region for Estimation of Density and Affinity: Graphical analysis based on the Scatchard plot (Scatchard, 1949) has been used to estimate the values of B_{max} and K_d from as series of PET recordings with various molar amounts of administered ligand (Farde *et al*, 1986). In brief, the ratios (B/F) of specific bound ligand concentration (B [pmol/mL]) and free ligand concentration (F [pmol/mL]) at equilibrium are plotted versus B. In this plot, the slope and *x*-intercept represent $-1/K_d$ and B_{max}, respectively. In general, for graphical analysis without arterial blood sampling, the total radioligand concentration in the reference region (C_r [Bq/mL]), where specific bindings are negligible, is used as an estimate of the free radioligand concentration in the target region (C_f [Bq/mL]), that is $C_f^{ref}=C_r$, and the specific binding radioligand concentration in the target region (C_b [Bq/mL]) is defined as radioactivity in the target region (C_t [Bq/mL]) reduced with C_r, that is $C_b^{ref}=C_t-C_r$ (Figure 1). The radioactivity concentrations of C_f^{ref} and C_b^{ref}, at the point in time when dC_b^{ref}/dt is 0 (T_{eq}), are divided by a specific activity of the administered ligand, and used as F and B at the transient equilibrium in the graphical analysis

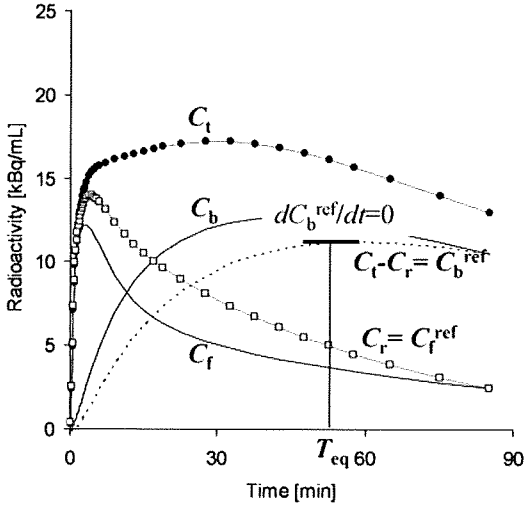

Figure 1 An example of simulated TACs for the striatum (C_t), free (C_f), and specific bound (C_b) concentrations in the striatum, the cerebellum used as a reference region (C_r) and bound concentration in the striatum estimated using a reference region ($C_b^{ref}=C_t-C_r$) with $K_1=0.033$, $K_1/k_2=0.59$, $k_{on}=0.0033$, $B_{max}=25.7$, $k_4=0.034$ for the striatum, and $K_1=0.034$, $K_1/k_2=0.36$, $k_3=0.022$, $k_4=0.034$ for the cerebellum. The time point of $dC_b^{ref}/dt=0$ (T_{eq}) is considered the transient equilibrium, and bound concentration at the equilibrium (B^{ref}) is obtained from the radioactivity concentration of C_b^{ref} at T_{eq}.

(Farde *et al*, 1989). In our study, we use the nomenclature B^{ref} and F^{ref} to represent the concentrations otherwise known as B and F. The value of the y axis, B^{ref}/F^{ref}, is sometimes replaced by the binding potential estimated by the graphical analysis of Logan *et al* (1996) or some other method (Logan *et al*, 1997; Doudet and Holden, 2003; Doudet *et al*, 2003).

Multiple-Injection Simplified Reference Tissue Model for Estimation of Binding Potential: A simplified reference tissue model (SRTM) can provide three parameters (R_1, k_2, BP_{ND}) without invasive arterial blood sampling by using a TAC of the reference region (Lammertsma and Hume, 1996). The MI-SRTM extended this SRTM for sequential multiple injections in a single session of PET scanning by taking into account the residual radioactivity in the target tissue at the time of each injection. As such, the magnitude of BP_{ND} for the ith injection is described in the following terms (Ikoma *et al*, 2009):

$$C_{ti}(t) = R_{1i}C_{ri}(t) + \left(k_{2i} - \frac{R_{1i}k_{2i}}{1+\mathrm{BP}_{NDi}}\right)e^{-\frac{k_{2i}}{1+\mathrm{BP}_{NDi}}t} \otimes C_{ri}(t) + (C_{ti}(0) - R_{1i}C_{ri}(0))e^{-\frac{k_{2i}}{1+\mathrm{BP}_{NDi}}t} \quad (1)$$

where C_{ti} and C_{ri} are the radioactivity concentrations in the target and reference region, respectively, and t is the time from the start of the ith injection.

Multiple-Injection Graphical Analysis for Estimation of Density and Affinity: The conventional graphical analysis was applied to the B_{max} and K_d estimations with the multiple-injection approach. In this multiple-injection graphical analysis (MI-GA), the BP_{ND} calculated for each injection using MI-SRTM was plotted as a function of the concentration of specific bound raclopride at the transient equilibrium (B^{ref} [pmol/mL]) within the scan duration for each injection, and B_{max} and K_d were estimated from the regression line.

In this study for [^{11}C]raclopride, the TAC of the cerebellum was used as the reference TAC. Each parameter in the MI-SRTM was estimated by nonlinear least squares fitting with iteration of the Gauss–Newton algorithm. It should be noted that the transient equilibrium condition is required for each injection in the MI-GA.

Simulation Analysis

Simulations were performed to determine the range of administered mass of three injections and to evaluate feasibility of the MI-GA to estimate the B_{max} and K_d.

Effect of Injected Mass on BP_{ND} Estimates: To investigate the effect of the administered molar amount of [^{11}C]raclopride on BP_{ND} estimates and to determine the molar amount of three injections for monkey studies, a relationship between BP_{ND} and B^{ref} was obtained by a computer simulation. Noiseless TACs of the striatum and cerebellum were generated with a measured plasma TAC and assumed parameter values derived from measurements taken from the monkey studies. The TAC of the cerebellum was simulated with a conventional two-tissue compartment four-parameter model with assumed parameter values obtained earlier in our monkey studies: $K_1 = 0.034$ (mL/mL/min) $K_1/k_2 = 0.36$, $k_3 = 0.022$ (min^{-1}), $k_4 = 0.034$ (min^{-1}). Meanwhile, the TAC of the striatum was simulated with a two-tissue compartment five-parameter model expressed as Equation (2) by solving these differential equations with the numerical analysis of fourth-order Runge–Kutta method with assumed parameter values $K_1 = 0.033$ (mL/mL/min), $K_1/k_2 = 0.59$, $k_{on} = 0.0033$ (mL/pmol/min), $B_{max} = 25.7$ (pmol/mL), $k_4 = 0.026$ (min^{-1}), and SA = 37 (GBq/μmol):

$$\begin{aligned} \frac{dC_f}{dt} &= K_1 C_p(t) - \left(k_2 + k_3'(t)\right)C_f(t) + k_4 C_b(t) \\ \frac{dC_b}{dt} &= k_3'(t)C_f(t) - k_4 C_b(t) \\ k_3'(t) &= k_{on}\left(B_{max} - \frac{C_b(t)}{SA}\right) \end{aligned} \quad (2)$$

where C_f and C_b are the concentrations of radioactivity for free and specifically bound [^{11}C]raclopride in tissue, respectively; and SA is the specific activity of administered [^{11}C]raclopride.

As reference, the relationships between B^{ref} and BP_{ND} or B^{ref}/F^{ref} were investigated in the case of a single injection of [^{11}C]raclopride by varying injected mass. TACs of the striatum and cerebellum for the single injection with a 50 mins scan were generated using the measured plasma TAC of a single injection in which the input plasma TAC was amplified, such that the corresponding mass increased from 1 to 500 nmol per injection. In each simulated TAC, BP_{ND} values were estimated by the SRTM, and then, B^{ref}/F^{ref} and B^{ref} were calculated by the transient equilibrium with the cerebellum TAC.

Next, TACs of the striatum and cerebellum for three injections at 50 mins intervals were generated using the plasma TAC of three sequential injections in which the input plasma TAC was amplified so that the mass of the first and second injections would be 1.5 and 10 nmol/kg, and the mass of the third injection would be 1.5 to 150 nmol/kg. In each simulated TAC, BP_{ND} values were estimated by the MI-SRTM, and B^{ref}/F^{ref} and B^{ref} for the third injection was calculated by the transient equilibrium with the cerebellum TAC. The relationships between B^{ref} and BP_{ND} or B^{ref}/F^{ref} for the third injection were investigated, and compared with that for the single injection.

Estimation of B_{max} and K_d Values by the Multiple-Injection Graphical Analysis: The reliability of B_{max} and K_d estimates by the graphical analysis was investigated for the proposed sequential multiple-injection approach (single PET scan) and compared with that for the conventional nonsequential approach (three PET scans on different days, such that no residual mass remained). Noiseless TACs of the striatum and cerebellum were simulated using assumed parameters of the two-tissue compartment model mentioned above and the plasma input function for three injections in which the magnitude of each 'virtual' input function was adjusted so that the injection mass would be 1.5, 10, or 30 nmol/kg determined from the simulation study mentioned above, with 50 mins intervals as reported